Photocatalytic Carbon Dioxide Reduction by Copper Oxide Nanocluster-Grafted Niobate Nanosheets

Ge Yin,[†] Masami Nishikawa,[‡] Yoshio Nosaka,[‡] Nagarajan Srinivasan,[†] Daiki Atarashi,[†] Etsuo Sakai,[†] and Masahiro Miyauchi*[,†,§]

[†]Department of Metallurgy and Ceramics Science, Graduate School of Science and Engineering, Tokyo Institute of Technology, 2-12-1 Ookayama, Meguro-ku, Tokyo 152-8552, Japan, [‡]Department of Materials Science and Technology, Nagaoka University of Technology, 1603-1, Kamitomioka-machi, Nagaoka, Niigata 940-2188, Japan, and [§]Japan Science and Technology Agency (JST), 4-1-8 Honcho Kawaguchi, Saitama 332-0012, Japan

ABSTRACT Amorphous copper oxide (Cu(II)) nanoclusters function as efficient electrocatalysts for the reduction of carbon dioxide (CO_2) to carbon monoxide (CO). In addition to promoting electrocatalytic activity, Cu(II) nanoclusters act as efficient cocatalysts for CO_2 photoreduction when grafted onto the surface of a semiconductor (light harvester), such as niobate ($Nb_3O_8^-$) nanosheets. Here, the photocatalytic activity and reaction pathway of Cu(II)-grafted $Nb_3O_8^-$ nanosheets was investigated using electron spin resonance (ESR) analysis and isotope-labeled molecules ($H_2{}^{18}O$ and $^{13}CO_2$). The results of the labeling experiments demonstrated that under UV irradiation, electrons are extracted from water to produce oxygen ($^{18}O_2$) and then reduce CO_2 to produce ^{13}CO. ESR analysis confirmed that excited holes in the valence band of $Nb_3O_8^-$ nanosheets react with water, and that excited electrons in the conduction band of $Nb_3O_8^-$ nanosheets are injected into the Cu(II) nanoclusters through the interface and are involved in the reduction of CO_2 into CO. The Cu(II) nanocluster-grafted $Nb_3O_8^-$ nanosheets are composed of nontoxic and abundant elements and can be facilely synthesized by a wet chemical method. The nanocluster grafting technique described here can be applied for the surface activation of various semiconductor light harvesters, such as metal oxide and/or metal chalcogenides, and is expected to aid in the development of efficient CO_2 photoreduction systems.

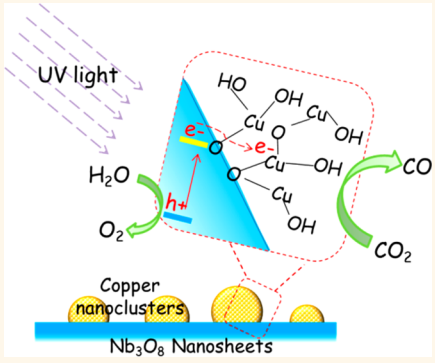

KEYWORDS: photocatalysis · electrocatalysis · CO_2 reduction · nanocluster · nanosheet · copper oxide · niobate

The need for safe and efficient solar energy conversion systems has been highlighted by current energy and environmental issues. In particular, photocatalytic carbon dioxide (CO_2) reduction has attracted increasing interest as an approach for directly converting solar energy to useful fuels, such as methane, methanol, carbon monoxide, formic acid and formaldehyde.[1,2] For such conversion, photocatalytic systems commonly consist of a photocatalytic semiconductor, termed a light harvester, coupled with a cocatalyst. Under light irradiation, excited electrons in the conduction band of the light harvester are injected into the cocatalyst to promote CO_2 reduction, while photogenerated holes in the valence band of the light harvester oxidize reducing agents, such as water molecules to produce oxygen. Since the finding that p-type gallium phosphide functions as a photocathode to convert aqueous carbon dioxide to formic acid, formaldehyde, and methanol, with part or all of the energy being supplied by light irradiation,[3] researches have focused on the identification of highly efficient light-harvesting materials. Several semiconductors, including TiO_2,[4] CdS, GaP, ZnO, SiC[5] and $SrTiO_3$,[6] have also been reported to be effective photocatalysts for CO_2 conversion. However, CO_2 photoreduction is generally considered to be more difficult than hydrogen evolution from water, as the former reaction requires high conduction band potential. Further, CO_2 reduction involves the multiple electrons

* Address correspondence to mmiyauchi@ceram.titech.ac.jp.

Received for review December 28, 2014 and accepted January 28, 2015.

Published online January 28, 2015
10.1021/nn507429e

reduction process; for example, two electrons for the production of carbon monoxide (CO) and formic acid (HCOOH), and six and eight electrons for methanol (CH_3OH) and methane (CH_4) production, respectively. Thus, the surface modification of light harvesters with cocatalyst is necessary to drive multielectron reduction reactions for the production of hydrocarbon fuels.

Recently, Sato *et al.* reported the photocatalytic reduction of CO_2 into formic acid with a quantum efficiency of 1.9% using N-doped Ta_2O_5 under visible light in the presence of ruthenium complex as a cocatalyst and triethanolamine as an electron donor.[7−9] Although ruthenium complex selectively promotes CO_2 reduction,[10] it is not an abundant material and requires a complicated synthesis process. In contrast to noble metal complexes, nanoparticles composed of metal or inorganic compounds such as copper,[11−13] silver,[14] and stannic oxide[15] are environmentally abundant and can be generated through facile synthesis reactions, and are therefore more suitable candidates as cocatalysts for practical CO_2 reduction systems. For example, silver (Ag)-loaded $ALa_4Ti_4O_{15}$ (A = Ca, Sr, or Ba) photocatalysts with layered perovskite structure efficiently produced more carbon monoxide than hydrogen using water as an electron donor.[14] In addition to the use of dispersed powder in photocatalytic reduction systems, the application of cathodic bias-potential for photoelectrochemical electrodes enables a negative potential shift to drive CO_2 reduction reactions.[15−17] To further lower the bias potential for selective reduction reactions, efficient cocatalysts are required. However, the development and combination of efficient CO_2 reduction cocatalysts with suitable light harvesters remains challenging.

An efficient CO_2 photoreduction system requires the following three components: (1) an efficient cocatalyst to drive multielectron reduction reactions by an electrochemical investigation under dark condition; (2) an effective light harvester modified with the cocatalyst for photocatalytic CO_2 reduction; and (3) the cocatalyst and light harvester materials must be derived from abundant and nontoxic elements. To satisfy the first and third requirements, various metallic electrocatalysts have been examined for CO_2 reduction.[18,19] In particular, copper is an abundant and eco-friendly element with high selectivity for CO and formic acid production[20−23] owing to its chemisorption−desorption of CO_2[24] and high CO binding energy.[25] Very recently, we reported that the grafting of cocatalysts composed of copper oxide (Cu(II)) nanoclusters onto TiO_2,[26−30] ZnO,[31,32] Bi_2O_3,[33] and $SrTiO_3$[34,35] as light harvesters efficiently promoted the multielectron reduction of oxygen molecules.[26−36] In these photocatalytic systems, the excited electrons are generated in the Cu(II) nanoclusters and react with oxygen molecules in a two-electron reduction reaction to produce hydrogen peroxide.[29,34] The small size of the Cu(II) nanoclusters (<3 nm) promotes the accumulation of excited electrons and thereby leads to the efficient multielectron reduction of oxygen. Further, the excited states of the nanoclusters are highly stable, as these Cu(II) nanoclusters are composed of amorphous oxides and exhibit high structural flexibility. Although Cu(II) nanoclusters have been used as cocatalysts for photocatalytic environmental purification, including antibacterial[30] and deodorization treatments,[26−28,30,33,35] their application for energy production, particularly water splitting and CO_2 photoreduction reactions, has not yet been reported. However, because many recent studies have demonstrated that metallic copper nanoparticles function as effective electrocatalysts for CO_2 reduction,[22,23,37−47] we speculated that Cu(II) nanoclusters are effective cocatalysts for multielectron reductions reactions in combination with light harvester compounds.

In contrast to cocatalysts, relatively few light harvesters are potentially applicable for CO_2 reduction, as the reaction requires more negative potential than that needed for hydrogen evolution or oxygen reduction. Among the various candidate, layered niobate compounds are expected to have sufficient negative conduction band potential for the reduction of CO_2 molecules.[48] In addition to the chemical composition, the quantum nanostructure of the light harvester markedly influences the conduction band level. We speculated that the conduction band of niobate could be increased according to quantum confinement effect[49] by delamination of bulk niobate to form nanosheet structures. This approach would also increase the specific surface area available for modification with cocatalysts and shorten the electron transport distance from the conduction band of the niobate ($Nb_3O_8^-$) nanosheets to the surface-grafted cocatalysts.

In the present research, we examined the electrocatalytic properties of Cu(II) nanoclusters grafted onto a conductive substrate under dark conditions with cathodic bias potential. After optimization of the cluster structure, the Cu(II) nanoclusters were grafted onto $Nb_3O_8^-$ nanosheet light harvester and the photocatalytic CO_2 reduction activities of the modified light harvester were investigated under UV-light irradiation. The dynamics of photogenerated charge carriers at the interface between the light harvester and nanocluster cocatalysts were investigated by spectroscopic analyses, including electron spin resonance (ESR), and the reaction pathway for CO_2 reduction was studied using an isotope labeling experiment.

RESULTS AND DISCUSSION

Electrocatalytic Property of Cu(II) Nanoclusters. Cu(II) nanoclusters were grafted onto a metal titanium substrate using an impregnation method[30] and their

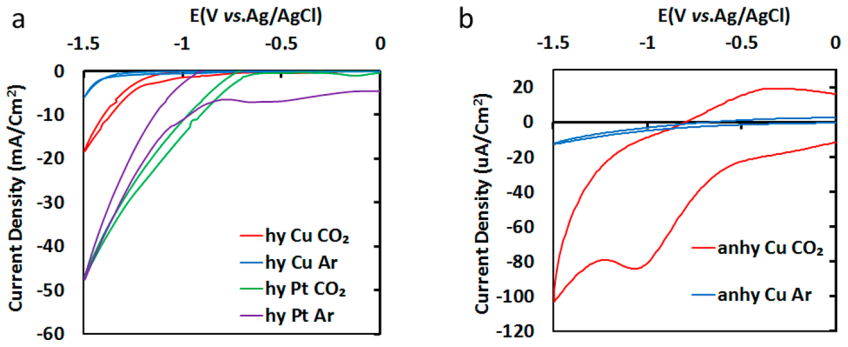

Figure 1. (a) Cyclic voltammograms of Ti sheets grafted with copper oxide nanoclusters or sputtered with platinum in aqueous electrolyte (0.5 M $KHCO_3$ for CO_2 bubbling, 0.5 M KCl for Ar bubbling; pH adjusted to 12 with NaOH). (b) Cyclic voltammograms of Ti sheets grafted with copper oxide nanoclusters in anhydrous organic electrolyte (acetonitrile containing 0.1 M tetraethylammonium tetrafluoroborate) under CO_2 or Ar bubbling.

electrocatalytic properties were then examined under CO_2 or Ar bubbling in aqueous and anhydrous conditions (Figure 1). As a comparison, an unmodified platinum plate was also examined as a representative conventional cathodic electrode. In an aqueous electrolyte, the platinum cathode exhibited a clear current generated from the water-splitting reaction, and no significant differences were observed between the CO_2 and Ar bubbling conditions (Figure 1a). In contrast, the current density of the electrode grafted with Cu(II) nanoclusters under a CO_2 atmosphere was higher than that under Ar bubbling. This current difference was assigned to the cathodic current generation of the reduction of CO_2 molecules and/or carbonic acid in water induced by the Cu(II) nanoclusters, as bare titanium substrate did not generate significant current differences under CO_2 or Ar bubbling. Under anhydrous electrolyte conditions, a similar trend was observed (Figure 1b), indicating that the Cu(II) nanoclusters acted as an effective electrocatalyst for CO_2 reduction.

X-ray photoelectron spectroscopy (XPS) analysis was conducted under electrochemical cathodic polarization to determine the valency of copper in each reduction peak (Figure S1a, Supporting Information). Without the application of bias potential (0 V), Cu(II) was detected, as indicated by the presence of high-intensity shakeup satellites at higher binding energy than the main $2p_{3/2}$ and $2p_{1/2}$ peaks,[50] which are not assigned to the spectra of Cu(0) and Cu(I). The satellite peaks of Cu(I) are similar to those of Cu(II) species, but the presence of Cu(I) was distinguished by the positive shift of the binding energy. Under a bias potential of −0.5 V (*vs* Ag/AgCl), Cu(II) ions were reduced to Cu(I). Under the bias potential of −1.2 V for several minutes, there is no XPS signal, indicating that the Cu(I) species are reduced to Cu(0) states, which are unstable and detached from the surface of the Ti electrode. We also evaluated the gas composition in the headspace of our electrochemical cell by gas chromatograph (Figure S1a, Supporting Information), then CO was detected under bias-potential at −0.5 V as well as −1.2 V. These results indicate that both the Cu(II) and Cu(I) species act as catalytic sites for the reduction of CO_2 into CO.

For the detailed structural characterization of the Cu(II) nanoclusters, we performed X-ray absorption near edge structure (XANES) and extended X-ray absorption fine structure (EXAFS) analyses using synchrotron apparatus (Figure S2, Supporting Information). The X-ray absorption analyses revealed that the local structures of the nanoclusters resembled copper monoxide (CuO) and/or copper hydroxide ($Cu(OH)_2$).[30,36] We also examined the Cu(II) nanoclusters grafted on the niobate nanosheet by transmission electron microscopy (TEM) (Figure 2d), and determined that the Cu(II) ion nanoclusters were several nanometers in size and had an amorphous structure. The Cu(II) nanoclusters on the niobate nanosheets were synthesized using a similar impregnation method to that used in our previous studies.[30] Previous studies have indicated that these amorphous copper oxides are highly stable under excited conditions and are critical for driving multielectron reduction reactions.[26−36]

Photocatalytic CO_2 Reduction with Cu(II) Nanoclusters as Cocatalyst. On the basis of the results of the above electrochemical experiments, Cu(II) nanoclusters appear to drive CO_2 reduction by lowering the bias potential. Therefore, the Cu(II) nanoclusters were expected to act as cocatalysts when grafted onto a light harvester, such as niobate nanosheets, with high conduction band potential. As revealed by atomic force microscopy (AFM), the prepared $Nb_3O_8^-$ nanosheets had monodispersed sheet morphology with a thickness below 2 nm, and length and width of hundreds of nanometers (Figure 2a). The same nanosheet morphologies were also observed by TEM analysis (Figure 2b). The obtained TEM diffraction pattern revealed that the $Nb_3O_8^-$ nanosheets had single crystal structure and that the exposed plane was oriented in the [010] direction (Figure 2c). The X-ray diffraction pattern of a thin film of $Nb_3O_8^-$ nanosheets clearly indicated

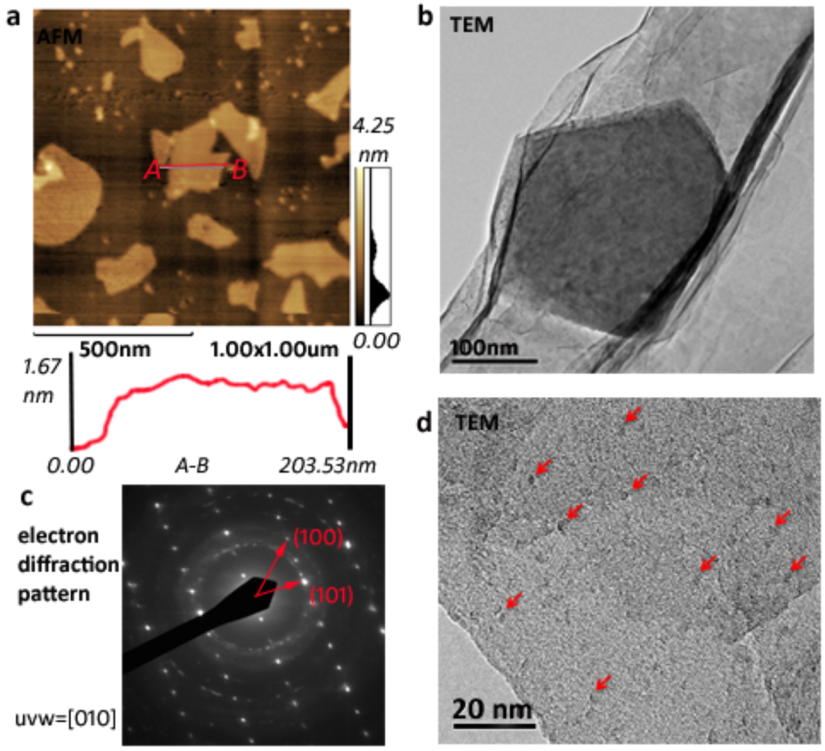

Figure 2. (a) AFM image, (b) TEM image, (c) and electron diffraction pattern of $Nb_3O_8^-$ nanosheets (L = 50 cm), and (d) TEM image of 2.5 wt % copper oxide nanoclusters-grafted $Nb_3O_8^-$ nanosheets.

that the crystals were oriented in the *b*-axis direction (Figure S3, Supporting Information), as the exposed faces of the $Nb_3O_8^-$ nanosheets were attached and stacked on each other. Figure 2d shows a TEM image for the Cu(II) nanocluster-grafted $Nb_3O_8^-$ nanosheets. Nanoclusters of 2−3 nm in size were clearly detected by energy dispersive X-ray spectroscopy (EDS, Figure S4, Supporting Information), and were found to be highly dispersed on the surface of the $Nb_3O_8^-$ nanosheets.

UV−visible absorption spectra were obtained for $Nb_3O_8^-$ nanosheets grafted with and without copper oxide nanoclusters (Figure 3a). The band-to-band transition of the $Nb_3O_8^-$ nanosheets appeared at 300 nm, whereas the absorption at 430 nm is attributable to interfacial charge transfer (IFCT).[30] The broad absorption in the range of 600−800 nm is attributable to the d-d transition of the Cu(II) species.[51] A plot of the square root of absorption efficiency (α) multiplied by the photon energy ($(\alpha h\nu)^{1/2}$) *versus* the photon energy showed a linear relationship (Figure 3b), indicating that the $Nb_3O_8^-$ nanosheet is an indirect transition-type semiconductor. The bandgap of the $Nb_3O_8^-$ nanosheets was estimated to be 3.56 eV, as calculated from the intersection of the plotted line of $(\alpha h\nu)^{1/2}$ *versus* photon energy with the abscissa axis.

For photocatalytic evaluation, the copper oxide nanoclusters-grafted $Nb_3O_8^-$ nanosheets (100 mg photocatalyst consisting of 10 wt % copper oxide nanoclusters was used in each experiment) were

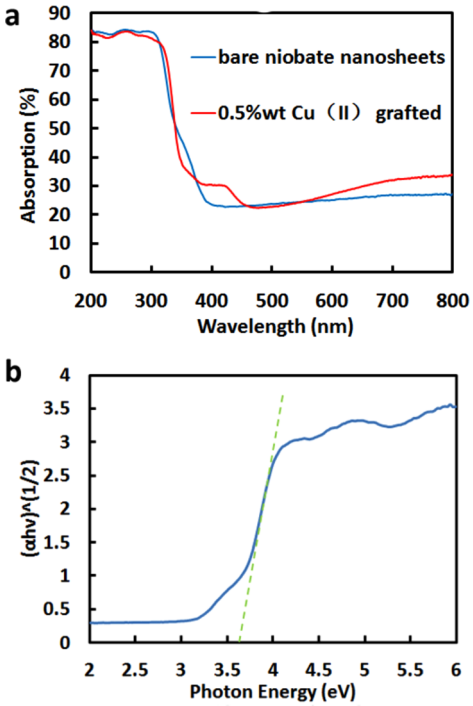

Figure 3. (a) UV−vis spectra of bare and 0.5 wt % copper oxide nanoclusters-grafted $Nb_3O_8^-$ nanosheets. (b) Plot of $(\alpha h\nu)^{1/2}$ *versus* photon energy for $Nb_3O_8^-$ nanosheets.

dispersed in gas-purged electrolyte (0.5 M $KHCO_3$ for CO_2 atmosphere and 0.5 M KCl for Ar atmosphere, adjusted to pH 12 with NaOH) and irradiated with UV light from a Xe−Hg lamp (Figure 4; the incident

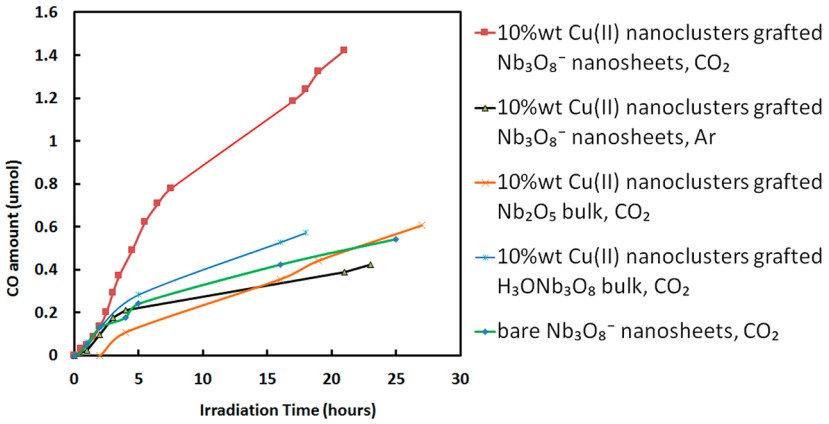

Figure 4. Time course of carbon monoxide generated by UV irradiation of copper oxide nanoclusters-grafted $Nb_3O_8^-$ nanosheets and control groups.

light spectrum is shown in Figure S5, Supporting Information). The gas-phase products in the headspace of the reactor were detected by gas chromatography (flame ionization detector (FID), with methanizer apparatus) and were found to be mainly composed of CO. Three control groups, consisting of bare $Nb_3O_8^-$ nanosheets, Cu(II) grafted bulk Nb_2O_5, and Cu(II) grafted bulk $H_3ONb_3O_8$ before delamination, were also included in the analysis to examine the effect of the grafted copper oxide nanoclusters and the nanosheet structure of niobate on CO generation. CO molecules were generated by each sample even under Ar bubbling, a result that was attributable to the oxidation of surface contaminants on the niobate nanosheets. However, CO generation was very limited on the bare $Nb_3O_8^-$ nanosheets under CO_2 or Ar bubbling (Figure S6, Supporting Information), indicating that the niobate nanosheet itself did not have photocatalytic CO_2 reduction activity. The reason for this lack of activity was considered to be the lack of reaction sites, as the negatively charged surfaces of $Nb_3O_8^-$ nanosheets limited CO_2 absorption. Nb_2O_5 and $H_3ONb_3O_8$ powders grafted with copper oxide nanoclusters were also photocatalytically evaluated as a comparison, and their activities were found to be much lower than that of the Cu(II)-modified $Nb_3O_8^-$ nanosheets, suggesting that the high conduction band level resulting from the quantum confinement effect is critical for driving CO_2 photoreduction.

During the photocatalytic evaluation, changes in the color of the copper oxide nanoclusters-grafted $Nb_3O_8^-$ nanosheets were observed. Under UV-light irradiation, the material changed from a light blue to musty green color within 1 h, indicating a change in the valency of copper. The results of XPS analysis (Figure S7, Supporting Information) indicated that a proportion of the Cu(II) ions were reduced to Cu(I) in response to UV-light irradiation. Notably, the reaction rate of the Cu(II) nanoclusters-grafted $Nb_3O_8^-$ nanosheets was not linear with respect to UV irradiation time, but rather, accelerated under light irradiation. This phenomenon was associated with the color change of the material. In the initial phase of UV irradiation, a portion of the Cu(II) ions in the nanoclusters are reduced to Cu(I), resulting in a mixture of Cu(II)/Cu(I) ions. The present experimental results suggest that the mixture of Cu(II)/Cu(I) species leads to efficient reduction of CO_2.

The redox potential of Cu(II)/Cu(I) ions is +0.16 V (*versus* NHE at pH = 0), which is more positive than that of the two-electron reduction of CO_2/CO. However, the conduction band of the $Nb_3O_8^-$ nanosheet synthesized in the present study is −1.32 V *vs* Ag/AgCl,[49] which is much more negative than the redox potential of CO_2/CO in the liquid phase (−0.52 V *vs* NHE at 25 °C, pH 7.0).[18] During UV-light irradiation, excited electrons in the conduction band of $Nb_3O_8^-$ nanosheet are injected into the Cu(II) nanoclusters, leading to a negative shift of the Fermi level of the nanoclusters. This shift allows the reduction of CO_2 into CO in response to UV irradiation. We also evaluated the photocatalytic activity of the Cu(II)-grafted $Nb_3O_8^-$ nanosheets under visible-light irradiation using a UV cutoff filter. However, negligible activity was detected under visible light, even though the Cu(II)-grafted $Nb_3O_8^-$ nanosheet absorbs visible light by d-d transition and IFCT.[30] These results indicate that the excitation of electrons to a sufficiently high conduction band level and the modification of the $Nb_3O_8^-$ nanosheet with cocatalysts are indispensable to drive photocatalytic CO_2 reduction. We attempted to optimize the photocatalytic activity of the Cu(II)-grafted $Nb_3O_8^-$ nanosheet by modifying the loading amount of the copper catalysts and the pH of the electrolyte. The optimal photocatalytic activity for CO_2 reduction was observed for $Nb_3O_8^-$ nanosheets grafted with 0.5 wt % copper oxide nanoclusters and dispersed in 0.5 M $KHCO_3$ solution (pH 12), as shown in Figure S8 of the Supporting Information.

Isotope Tracer and ESR Analyses. To verify oxygen generation and CO formation resulting from CO_2

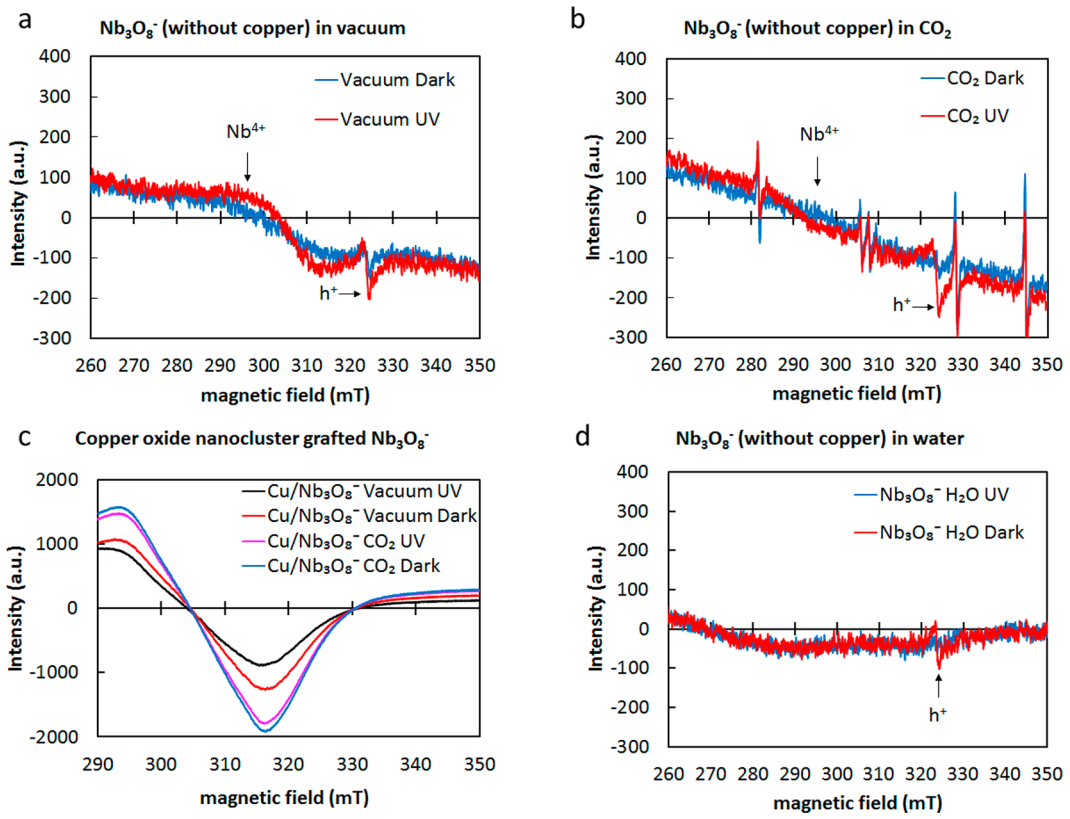

Figure 5. ESR spectra of bare niobate nanosheets in (a) vacuum, (b) CO_2, and (d) water. (c) ESR spectra of copper ion nanoclusters-grafted niobate nanosheets in the gas phase.

reduction, isotope tracer analyses involving $H_2{}^{18}O$ and $^{13}CO_2$ were conducted for the optimized Cu(II)-$Nb_3O_8^-$ nanosheet photocatalyst. Supporting Information Figure S9a shows the mass chromatography spectra for UV-irradiated $Nb_3O_8^-$ nanosheets grafted with 0.5 wt % copper oxide nanoclusters in 0.5 M $KHCO_3$/$H_2{}^{18}O$ solution purged with $^{12}CO_2$. A clear peak for $^{18}O_2$ (m/z = 36) was observed and continued to increase in size with increasing irradiation time. Supporting Information Figure S9b shows the mass chromatography spectra for UV-irradiated copper oxide nanoclusters-grafted $Nb_3O_8^-$ nanosheets in 0.01 M NaOH/$H_2{}^{16}O$ solution purged with $^{13}CO_2$, in which a peak corresponding to ^{13}CO (m/z = 29) was also detected. Together, these results confirmed that the CO detected during these photocatalytic reactions above was produced from CO_2 reduction and that the oxygen was generated from the oxidation of water.

Next, electron spin resonance (ESR) spectra measured under CO_2 atmosphere and vacuum conditions were used to determine the reaction route of the photoelectrons and holes generated during the UV-light irradiation of the copper oxide nanoclusters-grafted $Nb_3O_8^-$ nanosheets (Figure 5). The ESR spectra of bare $Nb_3O_8^-$ nanosheets before and after UV-light irradiation under vacuum or CO_2 atmosphere are shown in Figure 5, panels a and b, respectively. The broad signal appeared around 295 mT, which was assigned to surface Nb^{4+} ions that were generated by reaction with photoelectrons after UV irradiation, decreased in CO_2 atmosphere as compared to vacuum conditions, indicating that the photoelectrons in the conduction band of niobate nanosheets have sufficiently high potential to reduce CO_2, which would thus regenerate Nb^{5+} ions. Even though these ESR results indicate that the conduction band of $Nb_3O_8^-$ nanosheet has enough high potential to reduce CO_2 to some anion radical species, our experimental results revealed that bare $Nb_3O_8^-$ nanosheets did not generate CO molecules. These results also suggest that modification of Cu(II) nanoclusters onto niobate nanosheets light harvester is necessary to promote chemical reactions, including CO production.

In addition to the ESR analysis under gaseous conditions, we measured difference ESR spectra before and after UV-light irradiation in pure water (Figure 5d). Under vacuum conditions, photogenerated holes were detected as O^- species around 325 mT, which were assigned to the excited holes in the valence band of the O-2p orbital. In CO_2 atmosphere, the intensity of the excited holes increased because the consumption of the photoelectrons kept the existence of holes more stable. However, the intensity of the excited holes decreased under aqueous conditions, suggesting that the photogenerated holes in the valence band of $Nb_3O_8^-$ nanosheets are able to oxidize water to

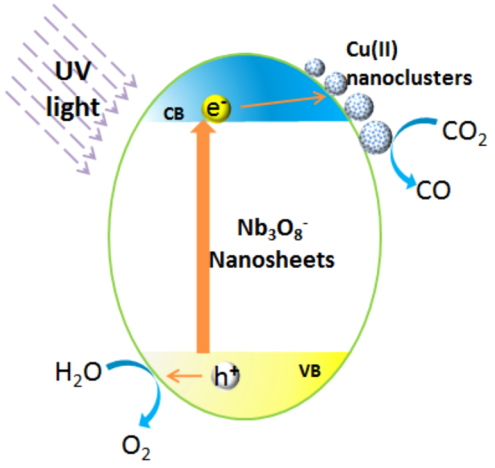

Figure 6. Schematic electronic structure of copper ion nanoclusters-grafted niobate nanosheet.

produce oxygen molecules. These results are consistent with the results of the isotope tracing experiment. To examine the role of the Cu(II) nanoclusters, Figure 5c) shows ESR difference spectra before and after UV-light irradiation of the Cu(II)-grafted $Nb_3O_8^-$ nanosheets. The d-orbital of Cu(II) species contains nine electrons; thus, an unpaired electron contributes to ESR signal. In contrast, Cu(I) is inactive for ESR. After UV-light irradiation of the Cu(II)-grafted $Nb_3O_8^-$ nanosheet in vacuum, the ESR signal of Cu(II) decreased, indicating that the excited electrons of the $Nb_3O_8^-$ nanosheet were injected into the Cu(II) nanoclusters. However, the ESR signal kept stable under CO_2 atmosphere, as the excited electrons in the Cu(II) nanoclusters were trapped by CO_2 molecules. The ESR analysis results strongly indicates that electrons are extracted from water molecules, excited by photon energy, and then injected into the Cu(II) nanoclusters, which are highly active sites for the production of CO molecules.

A proposed scheme of the photocatalytic process that occurs on the Cu(II) nanoclusters-grafted $Nb_3O_8^-$ nanosheet is shown in Figure 6. Under UV-light irradiation, electrons in the valence band of the $Nb_3O_8^-$ nanosheet are excited to the conduction band and then injected into the Cu(II) nanoclusters, as demonstrated by the ESR and XPS analyses, and the observed color change during the light irradiation. Photogenerated holes in the valence band of the $Nb_3O_8^-$ nanosheet then react with water to produce oxygen molecules, as was confirmed by the results of the isotope tracer analysis. The injected electrons reduce CO_2 to produce CO in a chemical reaction that was confirmed by the ESR spectral and isotope CO generation analyses. This is the first report to demonstrate that Cu(II) nanoclusters act as efficient cocatalysts for the multielectron reduction of CO_2. Cu(II) nanoclusters can be easily grafted onto any metal oxide semiconductor light harvester using a simple and economical impregnation method in aqueous medium. Although the photocatalyst constructed here functions under UV-light irradiation, it is expected that the present approach for the grafting of cocatalysts onto semiconductors can be applied toward the generation of visible-light harvesting material.

CONCLUSIONS

Using an elemental strategy and electrochemical-based investigation, we identified that amorphous Cu(II) nanoclusters function as efficient cocatalysts for the electrocatalytic reduction of CO_2 to CO. Using a soft-chemical method, we synthesized $Nb_3O_8^-$ nanosheets as a light harvesting material, which was found to have high conduction band potential because of the quantum confinement effect. The grafting of Cu(II) nanocluster cocatalysts onto the $Nb_3O_8^-$ nanosheets led to the efficient reduction of CO_2 molecules to CO under UV-light irradiation. Detailed ESR spectroscopic analysis and isotope labeling experiments demonstrated that electrons are extracted from water molecules and then excited by photon energy, which promotes their injection into Cu(II) nanoclusters, those are highly active sites for producing CO molecules. Notably, Cu(II) nanoclusters are composed of resource abundant and nontoxic elements, and can be easily deposited onto various metal oxide and/or metal chalcogenide light harvesters in mild aqueous media. The approach used in the present study for the grafting of cocatalytic nanoclusters is expected to be applicable for the development of efficient artificial photosynthesis systems.

MATERIALS AND METHODS

Fabrication of Copper Oxide Nanocluster-Modified Electrode. The grafting of copper oxide nanoclusters onto titanium (Ti) metal sheets used as the electrode was performed by an impregnation method, as previously described.[26,28,30] Briefly, Ti sheets ($0.1 \times 200 \times 200$ mm^3; Nirako Corp.) were cleaned by ultrasonication sequentially in nonphosphate detergent, distilled water (3 times), and ethanol, and were then immediately dried using a nitrogen gas gun. Polytetrafluoroethylene tape was affixed to the entire reverse surfaces of the Ti sheet and was used to surround a 1×1 cm^2 area on the front side of the sheet. For the grafting of Cu(II) nanoclusters, two Ti sheets were placed into 47.9 mL of distilled water heated to 90 °C in a vial reactor. A total of 1.6 mL of a 0.01 M $CuCl_2$ solution, which was prepared from $CuCl_2 \cdot 2H_2O$ as the source of Cu(II), was immediately added to the vial and 0.5 mL of 1 M NaOH was then added to adjust the pH to 12. The temperature of the solution was kept at 90 °C with stirring for 1 h. The grafted Ti sheets were then removed from the vials and immediately dried using a nitrogen gas gun.

Synthesis of $Nb_3O_8^-$ Nanosheets. Niobate nanosheets were prepared by delaminating bulk niobate with tetrabutylammonium hydroxide (TBAOH) using a soft-chemical procedure, as previously described.[49,52] Briefly, 1.01 g (0.01 mol) KNO_3 and 3.987 g (0.015 mol) Nb_2O_5 (molar ratio of 2:3) were mixed and ground with an agate mortar into a fine powder, which was then heated

to 900 °C over a 3-h period, and then held at 900 °C for 20 h. Approximately 0.001 mol (0.45 g) of the obtained KNb_3O_8 was placed into centrifuge tubes and mixed with 40 mL of 2.0 M HNO_3 aqueous solution for acid exchange. KNb_3O_8 was converted into $HNb_3O_8 \cdot 2H_2O$ by repeating the acid exchange three times. The centrifuge tubes were then centrifuged to remove the acid solution, and the obtained pellet was washed with distilled water until the supernatant reached neutral pH. The protonic oxide was delaminated into colloidal $Nb_3O_8^-$ nanosheets by reaction with an aqueous solution of tetrabutylammonium hydroxide (TBAOH) at a molar ratio 1:1 for about 10 days with continuous shaking. The suspension of $Nb_3O_8^-$ nanosheets was gently washed with sufficient amounts of weak HNO_3 solution during vacuum filtration using a membrane filter (0.025 μm; Millipore), and the filter containing the $Nb_3O_8^-$ nanosheets was then irradiated with black light in humid air to decompose the organic residue on the surface of $Nb_3O_8^-$ nanosheet powder.

Grafting Copper Oxide Nanoclusters onto the Surface of $Nb_3O_8^-$ Nanosheets. The grafting method for semiconductor powders is similar to the method for producing electrodes, but the amount of Cu(II) used for loading was increased from 0.5 to 10 wt %.

Electrochemical Evaluation. For electrochemical evaluation, Cu(II) nanoclusters were grafted on the surface of the Ti sheets used as working electrodes. The electrodes were placed in electrolyte solution (0.5 M $KHCO_3$ for CO_2 bubbling and 0.5 M KCl for Ar bubbling; both adjusted to pH 12 with NaOH) inside a closed glass cell and the electrolyte was then bubbled with CO_2 or Ar gas to create different atmospheres. The electrocatalytic properties of the grafted electrodes were evaluated by comparing the cyclic voltammogram curves obtained under CO_2 or Ar bubbling. To confirm that the observed differences were due to the reduction of CO_2 rather than water splitting, cyclic voltammogram curves were also measured for electrodes placed in an anhydrous organic electrolyte (acetonitrile containing 0.1 M tetraethylammonium tetrafluoroborate). Ti sheets sputtered with platinum (~50 nm) were used as a control to demonstrate the selectivity for CO_2 reduction, as platinum is a well-known electrocatalyst for water splitting.

Photocatalytic Evaluation. The prepared powders were dispersed in 20 mL of electrolyte (0.5 M $KHCO_3$ aqueous solution, adjusted to pH 12 with NaOH) in a Petri dish, which was then placed into a sealed glass reactor (500 mL) covered with a quartz glass cap. CO_2 or Ar gas was bubbled inside of the reactor through silica tubes at a flow rate of 100 mL/min for 30 min to create a saturated atmosphere of CO_2 or Ar. The reactor was irradiated by UV light (Hg−Xe lamp (240−300 nm), LA-410UV, Hayashi), and products in the headspace were collected by a syringe and then injected into gas chromatograph (flame ionization detector (FID) equipped with a methanizer apparatus) to detect CO and methane.

Isotope Experiments. Isotope experiments were performed in a rectangle quartz glass cell ($1 \times 1 \times 5$ cm^3). The cells were irradiated with the same UV lamp used in the photocatalytic evaluations, and products in the headspace of the quartz glass cells were detected by gas chromatography (GC)−mass spectrometry (MS) (Shimadzu). All isotope chemicals were purchased from Isotec-Sigma-Aldrich.

Conflict of Interest: The authors declare no competing financial interest.

Acknowledgment. This work has been supported by a grant from Advanced Catalytic Transformation program for Carbon utilization (ACT-C), Japan Science and Technology Agency (JST). We thank Dr. K. Kamiya, Tokyo University, for the XANES and EXAFS measurements performed at SPring-8. We also thank Mr. A. Genseki and Mr. K. Hori at the Center for Advanced Materials Analysis for help with the TEM characterization, and also acknowledge Mr. Greg Newton for the critical reading of the manuscript. G. Yin and M. Miyauchi proposed the concept. G. Yin acquired experimental data. M. Nishikawa and Y. Nosaka performed the ESR analysis. N. Srinivasan, D. Atarashi, and E. Sakai gave important suggestions. G. Yin and M. Miyauchi wrote the manuscript. M. Miyauchi conceived the project.

Supporting Information Available: XPS analysis of the Cu in the copper oxide nanoclusters during electrochemical evaluation under different bias potentials; XANES and EXAFS of Cu; XRD patterns of niobate nanosheets; elemental analysis of the copper oxide nanoclusters-grafted niobate nanosheets by TEM equipment; spectrum of incident light used in the photocatalytic evaluation; photocatalytic performance of bare niobate nanosheets; XPS analysis of the Cu(II)-$Nb_3O_8^-$ nanosheets under UV irradiation; optimization of the cocatalyst loading amount and electrolyte pH; results of the isotope experiments. This material is available free of charge *via* the Internet at http://pubs.acs.org.

REFERENCES AND NOTES

1. Habisreutinger, S. N.; Schmidt-Mende, L.; Stolarczyk, J. K. Photocatalytic Reduction of CO_2 on TiO_2 and Other Semiconductors. *Angew. Chem., Int. Ed.* **2013**, *52*, 7372–7408.
2. Tran, P. D.; Wong, L. H.; Barber, J.; Loo, J. S. Recent Advances in Hybrid Photocatalysts for Solar Fuel Production. *Energy Environ. Sci.* **2012**, *5*, 5902–5918.
3. Halmann, M. Photoelectrochemical Reduction of Aqueous Carbon Dioxide on p-Type Gallium Phosphide in Liquid Junction Solar Cells. *Nature* **1978**, *275*, 115–116.
4. In, S.-I.; Vaughn, D. D.; Schaak, R. E. Hybrid CuO-TiO_2-xNx Hollow Nanocubes for Photocatalytic Conversion of CO_2 into Methane under Solar Irradiation. *Angew. Chem., Int. Ed.* **2012**, *51*, 3915–3918.
5. Inoue, T.; Fujishima, A.; Konishi, S.; Honda, K. Photoelectrocatalytic Reduction of Carbon Dioxide in Aqueous Suspensions of Semiconductor Powders. *Nature* **1979**, *277*, 637–638.
6. Halmann, M.; Ulman, M.; Aurian-Blajeni, B. Photochemical Solar Collector for the Photoassisted Reduction of Aqueous Carbon Dioxide. *Sol. Energy* **1983**, *31*, 429–431.
7. Sato, S.; Morikawa, T.; Saeki, S.; Kajino, T.; Motohiro, T. Visible-Light-Induced Selective CO_2 Reduction Utilizing a Ruthenium Complex Electrocatalyst Linked to a p-Type Nitrogen-Doped Ta_2O_5 Semiconductor. *Angew. Chem., Int. Ed.* **2010**, *49*, 5101–5105.
8. Sato, S.; Arai, T.; Morikawa, T.; Uemura, K.; Suzuki, T. M.; Tanaka, H.; Kajino, T. Selective CO_2 Conversion to Formate Conjugated with H_2O Oxidation Utilizing Semiconductor/Complex Hybrid Photocatalysts. *J. Am. Chem. Soc.* **2011**, *133*, 15240–15243.
9. Suzuki, T. M.; Nakamura, T.; Saeki, S.; Matsuoka, Y.; Tanaka, H.; Yano, K.; Kajino, T.; Morikawa, T. Visible Light-Sensitive Mesoporous N-doped Ta_2O_5 Spheres: Synthesis and Photocatalytic Activity for Hydrogen Evolution and CO_2 Reduction. *J. Mater. Chem.* **2012**, *22*, 24584–24590.
10. Ishida, H.; Tanaka, K.; Tanaka, T. Electrochemical CO_2 Reduction Catalyzed by Ruthenium Complexes $[Ru(bpy)_2(CO)_2]^{2+}$ and $[Ru(bpy)_2(CO)Cl]^+$. Effect of pH on the Formation of CO and HCOO. *Organometallics* **1987**, *6*, 181–186.
11. Shown, I.; Hsu, H.-C.; Chang, Y. C.; Lin, C.-H.; Roy, P. K.; Ganguly, A.; Wang, C.-H.; Chang, J. K.; Wu, C.-I.; Chen, L.-C. Highly Efficient Visible Light Photocatalytic Reduction of CO_2 to Hydrocarbon Fuels by Cu-NPs Decorated Graphene Oxide. *Nano Lett.* **2014**, *14*, 6097–6103.
12. Ba, X.; Yan, L.-L.; Huang, S.; Yu, J.; Xia, X.-J.; Yu, Y. New Way for CO_2 Reduction under Visible Light by a Combination of a Cu Electrode and Semiconductor Thin Film: Cu_2O Conduction Type and Morphology Effect. *J. Phys. Chem. C* **2014**, *118*, 24467–24478.
13. Neaţu, Ş.; Maciá-Agulló, J. A.; Concepción, P.; Garcia, H. Gold-Copper Nanoalloys Supported on TiO_2 as Photocatalysts for CO_2 Reduction by Water. *J. Am. Chem. Soc.* **2014**, *136*, 15969–15976.
14. Iizuka, K.; Wato, T.; Miseki, Y.; Saito, K.; Kudo, A. Photocatalytic Reduction of Carbon Dioxide over Ag Cocatalyst-Loaded $ALa_4Ti_4O_{15}$ (A= Ca, Sr, and Ba) Using Water as a Reducing Reagent. *J. Am. Chem. Soc.* **2011**, *133*, 20863–20868.
15. Magesh, G.; Kim, E. S.; Kang, H. J.; Banu, M.; Kim, J. Y.; Kim, J. H.; Lee, J. S. A Versatile Photoanode-Driven Photoelectrochemical System for Conversion of CO_2 to Fuels with

High Faradaic Efficiencies at Low Bias Potentials. *J. Mater. Chem. A* **2014**, *2*, 2044–2049.
16. Noda, H.; Yamamoto, A.; Ikeda, S.; Maeda, M.; Ito, K. Influence of Light Intensity on Photoelectroreduction of CO_2 at a p-GaP Photocathode. *Chem. Lett.* **1990**, 1757–1760.
17. Barton, E. E.; Rampulla, D. M.; Bocarsly, A. B. Selective Solar-Driven Reduction of CO_2 to Methanol Using a Catalyzed p-GaP Based Photoelectrochemical Cell. *J. Am. Chem. Soc.* **2008**, *130*, 6342–6344.
18. Hori, Y., Electrochemical CO_2 Reduction on Metal Electrodes. *Modern Aspects of Electrochemistry*; Springer: New York, 2008; Vol. 42, pp 89−189.
19. Azuma, M.; Hashimoto, K.; Hiramoto, M.; Watanabe, M.; Sakata, T. Electrochemical Reduction of Carbon Dioxide on Various Metal Electrodes in Low-Temperature Aqueous $KHCO_3$ Media. *J. Am. Chem. Soc.* **1990**, *137*, 1772–1778.
20. Hara, K.; Kudo, A.; Sakata, T. Electrochemical Reduction of Carbon Dioxide under High Pressure on Various Electrodes in an Aqueous Electrolyte. *J. Electroanal. Chem.* **1995**, *391*, 141–147.
21. Satoshi Kaneco, K. I. K. O. T. M. Electrochemical CO_2 Reduction on a Copper Wire Electrode in Tetraethylammonium Perchlorate Methanol at Extremely Low Temperature. *Energy Source* **1999**, *21*, 643–648.
22. Reske, R.; Mistry, H.; Behafarid, F.; Roldan Cuenya, B.; Strasser, P. Particle Size Effects in the Catalytic Electroreduction of CO_2 on Cu Nanoparticles. *J. Am. Chem. Soc.* **2014**, *136*, 6978–6986.
23. Manthiram, K.; Beberwyck, B. J.; Alivisatos, A. P. Enhanced Electrochemical Methanation of Carbon Dioxide with a Dispersible Nanoscale Copper Catalyst. *J. Am. Chem. Soc.* **2014**, *136*, 13319–13325.
24. Copperthwaite, R. G.; Davies, P. R.; Morris, M. A.; Roberts, M. W.; Ryder, R. A. The Reactive Chemisorption of Carbon Dioxide at Magnesium and Copper Surfaces at Low Temperature. *Catal. Lett.* **1988**, *1*, 11–19.
25. Kuhl, K. P.; Hatsukade, T.; Cave, E. R.; Abram, D. N.; Kibsgaard, J.; Jaramillo, T. F. Electrocatalytic Conversion of Carbon Dioxide to Methane and Methanol on Transition Metal Surfaces. *J. Am. Chem. Soc.* **2014**, *136*, 14107–14113.
26. Liu, M.; Qiu, X.; Hashimoto, K.; Miyauchi, M. Cu (II) Nanocluster-Grafted, Nb-Doped TiO_2 as an Efficient Visible-Light-Sensitive Photocatalysts Based on Energy-Level Matching between Surface and Bulk States. *J. Mater. Chem. A* **2014**, *2*, 13571–13579.
27. Liu, M.; Inde, R.; Nishikawa, M.; Qiu, X.; Atarashi, D.; Sakai, E.; Nosaka, Y.; Hashimoto, K.; Miyauchi, M. Enhanced Photoactivity with Nanocluster-Grafted Titanium Dioxide Photocatalysts. *ACS Nano* **2014**, *8*, 7229–7238.
28. Liu, M.; Qiu, X.; Miyauchi, M.; Hashimoto, K. Cu (II) Oxide Amorphous Nanoclusters Grafted Ti^{3+} Self-Doped TiO_2: An Afficient Visible Light Photocatalyst. *Chem. Mater.* **2011**, *23*, 5282–5286.
29. Nosaka, Y.; Takahashi, S.; Sakamoto, H.; Nosaka, A. Y. Reaction Mechanism of Cu (II)-Grafted Visible-Light Responsive TiO_2 and WO_3 Photocatalysts Studied by Means of ESR Spectroscopy and Chemiluminescence Photometry. *J. Phys. Chem. C* **2011**, *115*, 21283–21290.
30. Qiu, X.; Miyauchi, M.; Sunada, K.; Minoshima, M.; Liu, M.; Lu, Y.; Li, D.; Shimodaira, Y.; Hosogi, Y.; Kuroda, Y. Hybrid Cu_xO/TiO_2 Nanocomposites as Risk-Reduction Materials in Indoor Environments. *ACS Nano* **2012**, *6*, 1609–1618.
31. Anandan, S.; Miyauchi, M. Ce-doped ZnO ($Ce_xZn_{1-x}O$) Becomes an Efficient Visible-Light-Sensitive Photocatalyst by Co-catalyst (Cu^{2+}) Grafting. *Phys. Chem. Chem. Phys.* **2011**, *13*, 14937–14945.
32. Anandan, S.; Ohashi, N.; Miyauchi, M. ZnO-Based Visible-Light Photocatalyst: Band-Gap Engineering and Multi-Electron Reduction by Co-catalyst. *Appl. Catal., B* **2010**, *100*, 502–509.
33. Hu, J.; Li, H.; Huang, C.; Liu, M.; Qiu, X. Enhanced Photocatalytic Activity of Bi_2O_3 under Visible Light Irradiation by Cu (II) Clusters Modification. *Appl. Catal., B* **2013**, *142*, 598–603.
34. Nosaka, Y.; Takahashi, S.; Mitani, Y.; Qiu, X.; Miyauchi, M. Reaction Mechanism of Visible-Light Responsive Cu(II)-Grafted Mo-Doped $SrTiO_3$ Photocatalyst Studied by Means of ESR Spectroscopy and Chemiluminescence Photometry. *Appl. Catal., B* **2012**, *111−112*, 636–640.
35. Qiu, X.; Miyauchi, M.; Yu, H.; Irie, H.; Hashimoto, K. Visible-Light-Driven Cu (II)-$(Sr_{1-y}Na_y)(Ti_{1-x}Mo_x)$ O_3 Photocatalysts Based on Conduction Band Control and Surface Ion Modification. *J. Am. Chem. Soc.* **2010**, *132*, 15259–15267.
36. Irie, H.; Kamiya, K.; Shibanuma, T.; Miura, S.; Tryk, D. A.; Yokoyama, T.; Hashimoto, K. Visible Light-Sensitive Cu(II)-Grafted TiO_2 Photocatalysts: Activities and X-ray Absorption Fine Structure Analyses. *J. Phys. Chem. C* **2009**, *113*, 10761–10766.
37. Baturina, O. A.; Lu, Q.; Padilla, M. A.; Xin, L.; Li, W.; Serov, A.; Artyushkova, K.; Atanassov, P.; Xu, F.; Epshteyn, A.; et al. CO_2 Electroreduction to Hydrocarbons on Carbon-Supported Cu Nanoparticles. *ACS Catal.* **2014**, *4*, 3682–3695.
38. Reske, R.; Duca, M.; Oezaslan, M.; Schouten, K. J. P.; Koper, M. T. M.; Strasser, P. Controlling Catalytic Selectivities during CO_2 Electroreduction on Thin Cu Metal Overlayers. *J. Phys. Chem. Lett.* **2013**, *4*, 2410–2413.
39. Calle-Vallejo, F.; Koper, M. T. M. Theoretical Considerations on the Electroreduction of CO to C_2 Species on Cu(100) Electrodes. *Angew. Chem., Int. Ed.* **2013**, *52*, 7282–7285.
40. Kauffman, D. R.; Ohodnicki, P. R.; Kail, B. W.; Matranga, C. Selective Electrocatalytic Activity of Ligand Stabilized Copper Oxide Nanoparticles. *J. Phys. Chem. Lett.* **2011**, *2*, 2038–2043.
41. Durand, W. J.; Peterson, A. A.; Studt, F.; Abild-Pedersen, F.; Nørskov, J. K. Structure Effects on the Energetics of the Electrochemical Reduction of CO_2 by Copper Surfaces. *Surf. Sci.* **2011**, *605*, 1354–1359.
42. Peterson, A. A.; Abild-Pedersen, F.; Studt, F.; Rossmeisl, J.; Norskov, J. K. How Copper Catalyzes the Electroreduction of Carbon Dioxide into Hydrocarbon Fuels. *Energy Environ. Sci.* **2010**, *3*, 1311–1315.
43. Li, C. W.; Kanan, M. W. CO_2 Reduction at Low Overpotential on Cu Electrodes Resulting from the Reduction of Thick Cu_2O Films. *J. Am. Chem. Soc.* **2012**, *134*, 7231–7234.
44. Schouten, K. J. P.; Qin, Z.; Gallent, E. P.; Koper, M. T. M. Two Pathways for the Formation of Ethylene in CO Reduction on Single-Crystal Copper Electrodes. *J. Am. Chem. Soc.* **2012**, *134*, 9864–9867.
45. Zhang, Y.-J.; Sethuraman, V.; Michalsky, R.; Peterson, A. A. Competition between CO_2 Reduction and H_2 Evolution on Transition-Metal Electrocatalysts. *ACS Catal.* **2014**, *4*, 3742–3748.
46. Kim, D.; Resasco, J.; Yu, Y.; Asiri, A. M.; Yang, P. Synergistic Geometric and Electronic Effects for Electrochemical Reduction of Carbon Dioxide Using Gold-Copper Bimetallic Nanoparticles. *Nat. Commun.* **2014**, *5*, 4948.
47. Friebel, D.; Mbuga, F.; Rajasekaran, S.; Miller, D. J.; Ogasawara, H.; Alonso-Mori, R.; Sokaras, D.; Nordlund, D.; Weng, T.-C.; Nilsson, A. Structure, Redox Chemistry, and Interfacial Alloy Formation in Monolayer and Multilayer Cu/Au(111) Model Catalysts for CO_2 Electroreduction. *J. Phys. Chem. C* **2014**, *118*, 7954–7961.
48. Scaife, D. Oxide Semiconductors in Photoelectrochemical Conversion of Solar Energy. *Sol. Energy* **1980**, *25*, 41–54.
49. Akatsuka, K.; Takanashi, G.; Ebina, Y.; Sakai, N.; Haga, M.-a.; Sasaki, T. Electrochemical and Photoelectrochemical Study on Exfoliated Nb_3O_8 Nanosheet. *J. Phys. Chem. Solids* **2008**, *69*, 1288–1291.
50. Arai, T.; Horiguchi, M.; Yanagida, M.; Gunji, T.; Sugihara, H.; Sayama, K. Reaction Mechanism and Activity of WO_3-Catalyzed Photodegradation of Organic Substances Promoted by A CuO Cocatalyst. *J. Phys. Chem. C* **2009**, *113*, 6602–6609.
51. Dias Filho, N. L. Adsorption of Cu(II) and Co(II) Complexes on a Silica Gel Surface Chemically Modified with 2-Mercaptoimidazole. *Microchim. Acta* **1999**, *130*, 233–240.
52. Katsumata, K.-i.; Okazaki, S.; Cordonier, C. E.; Shichi, T.; Sasaki, T.; Fujishima, A. Preparation and Characterization of Self-Cleaning Glass for Vehicle with Niobia Nanosheets. *ACS Appl. Mater. Interfaces* **2010**, *2*, 1236–1241.